Published in "Cytometry Part A 83(9): 794–805, 2013"
which should be cited to refer to this work.

Dynamic Conformational Transitions of the EGF Receptor in Living Mammalian Cells Determined by FRET and Fluorescence Lifetime Imaging Microscopy

Iwona Ziomkiewicz,[1†] Anastasia Loman,[2‡] Reinhard Klement,[1,3] Cornelia Fritsch,[1$] Andrey S. Klymchenko,[4] Gertrude Bunt,[2,5] Thomas M. Jovin,[1] Donna J. Arndt-Jovin[1*]

Iwona Ziomkiewicz and Anastasia Loman contributed equally to the work.
[1]Laboratory of Cellular Dynamics, Max Planck Institute for Biophysical Chemistry, 37077, Göttingen, Germany
[2]Department of Neuro- and Sensory Physiology, University Medicine Göttingen, 37075, Göttingen, Germany
[3]Department of Theoretical and Computational Biophysics, Max Planck Institute for Biophysical Chemistry, 37077, Göttingen, Germany
[4]Laboratoire de Biophotonique et Pharmacologie, UMR 7213 CNRS, Faculté de Pharmacie, Université de Strasbourg, 67401, France
[5]DFG Research Center Nanoscale Microscopy and Molecular Physiology of the Brain, Göttingen, Germany
[†]Present address of I.Z.: Department of Plant and Environmental Sciences, University of Copenhagen, 1871 Frederiksberg, Denmark.
[‡]Present address of A.L.: Centre d'Immunologie, Université Marseille-Luminey, Marseille, France.
[$]Present address of C.F.: Dept of Biology, University of Fribourg, 1700 Fribourg, Switzerland.
Research sponsor: Max Planck Society; DFG Center for the Molecular Physiology of the Brain (CMPB)
*Correspondence to: Donna J. Arndt-Jovin, Laboratory of Cellular Dynamics, Max Planck Institute for Biophysical Chemistry, 37077 Göttingen, Germany. E-mail: djovin@gwdg.de

Abstract

We have revealed a reorientation of ectodomain I of the epidermal growth factor receptor (EGFR; ErbB1; Her1) in living CHO cells expressing the receptor, upon binding of the native ligand EGF. The state of the unliganded, nonactivated EGFR was compared to that exhibited after ligand addition in the presence of a kinase inhibitor that prevents endocytosis but does not interfere with binding or the ensuing conformational rearrangements. To perform these experiments, we constructed a transgene EGFR with an acyl carrier protein sequence between the signal peptide and the EGFR mature protein sequence. This protein, which behaves similarly to wild-type EGFR with respect to EGF binding, activation, and internalization, can be labeled at a specific serine in the acyl carrier tag with a fluorophore incorporated into a 4′-phosphopantetheine (P-pant) conjugate transferred enzymatically from the corresponding CoA derivative. By measuring Förster resonance energy transfer between a molecule of Atto390 covalently attached to EGFR in this manner and a novel lipid probe NR12S distributed exclusively in the outer leaflet of the plasma membrane, we determined the apparent relative separation of ectodomain I from the membrane under nonactivating and activating conditions. The data indicate that the unliganded domain I of the EGFR receptor is situated much closer to the membrane before EGF addition, supporting the model of a self-inhibited configuration of the inactive receptor in quiescent cells.

Key terms

lifetime imaging; time-correlated single-photon counting; epidermal growth factor receptor; tethered configuration; EGF; FRET

The X-ray crystallographic structures of the extracellular domain of the epidermal growth factor receptor (EGFR) have been determined in both the liganded (1,2) and unliganded (3) states. In the structures with bound EGF or TGFα, the ligand is associated with an extended region comprising domains I and III, and a homodimeric structure is generated by interaction of β-hairpins protruding from the two domains II of the constituent monomers, confirming an earlier model of Lemmon et al. (4). This extended structure was also seen in the extracellular domain of the ErbB2 member of the ErbB family (5). ErbB2 lacks a known ligand but features a potent kinase domain requiring activation by its preferred heterodimerization partners EGFR and ErbB3. In contrast, the unliganded extracellular domain of EGFR crystallized in a self-inhibitory structure in which the domain II dimerization arm is completely suppressed by intramolecular interactions with domain IV (3). This structure has been presumed to be the form assumed by the inactive native receptor in the plasma membrane. A number of in vivo studies featuring mutated EGFR (6), antibody binding (7), and co-crystal structures of mAbs with native EGFR (8,9) have confirmed the

existence of a configuration in which the EGF-binding face of domain III is exposed. Lemmon (10) has suggested that EGFR be considered an allosteric enzyme, such that a complete understanding of the receptor requires combining cellular and structural studies. However, a recent study has challenged the existence of the inhibited conformation of the receptor in live cells. A chimeric full-length EGFR with YFP fused to its amino-terminus was reported to exclusively exist in the extended conformation both in the presence and absence of EGF (11).

We have addressed these issues by determining the orientation of the ectodomain of the full-length EGFR in quiescent cells compared to that exhibited after the addition of EGF. For these purposes, we constructed a new chimeric EGFR with an acyl carrier protein (ACP) tag fused to the wild-type amino terminus consisting of a three-helix bundle of 78 amino acids in which the serine in position 36 at the end of helix 2 served as the target for the enzymatic transfer by specific phosphopantetheine transferases (PPTases) of a fluorescent probe from the corresponding thiol-substituted CoA substrate. The ACP tag is a small entity of $\leq$7 kDa and is very versatile in terms of the labeling moiety, which can be a fluorophore, a quantum dot, or an affinity probe (12,13).

Stably transfected cell lines were established and used in this study. The mutated EGFR protein was expressed well in mammalian cells and inserted into the extracellular membrane. It exhibited the properties of wild-type EGFR; that is, the kinase was dormant in starved cells but the receptor-bound EGF was thereby activated normally, showing the kinetics of downstream signaling and endocytosis characteristic of native EGFR (see Supporting Information Figs. S1 and S2).

The mutated EGFR protein was labeled with a donor fluorophore Atto390, capable of excitation by a multiphoton fs Ti–Sapphire laser, and images were acquired by the TCSPC technique. It was anticipated that fluorescence of the donor on the ACP tag would be reduced by FRET to the NR12S lipid probe localized in the outer leaflet of the cell membrane (14). Based on molecular modeling predicting donor-membrane distances varying from ~6 to 12 nm (see Results section) and an R_o of 5.4 nm, it was anticipated that the FRET efficiency would vary significantly with the absence or presence of the EGF ligand, that is, conditions representing the quiescent or ligand-bound state, respectively. The experimental strategy is summarized in Figure 1.

Our data demonstrate significant differences in the distance of the amino terminus of EGFR to the plasma membrane in the unliganded and liganded states, supporting the model of a self-inhibited conformation of the unliganded receptor in the quiescent state.

Materials and Methods

Molecular Modeling

The models of EGFR with an attached ACP tag in the putative inhibited and activated conformations were constructed with PyMOL (16). The structures were energy-minimized and then subjected to short (10 ns) molecular dynamics (MD) runs to allow for a reorientation of the ACP with respect to the EGFR. The minimization and MD simulations were carried out on fully hydrated systems (TIP3P water) and 150 mM NaCl bulk salt concentration (Fig. 2). The amber99sb-ildn force-field (18) was used with GROMACS 4.55 (19). After these procedures, the Atto390 probe with its linker was attached to SER36 of the ACP (Fig. 2).

Chimeric ACP-EGFR Protein and Expression in Cells

We constructed a chimeric EGFR with an amino terminal acyl carrier protein tag (20) attached to the amino terminus of the mature human EGFR. The DNA sequence for the 78 amino acid sequence of the ACP tag was extracted from the AGA-plasmid (kind gift of N. Johnsson) by PCR and inserted between the DNA for the signal sequence and the amino terminus by creating a new Nhe1 restriction enzyme cleavage site using site-directed mutagenesis of wild-type EGFR in pcDNA3 or a modified pcDNA3.1zeo-plasmid. Stably transfected CHO cell lines were selected by antibiotic resistance and single-cell cloning. The serine that accepts the 4'-phosphopantetheine (P-pant) conjugate occurs at residue 36 in the sequence of the mature expressed protein. The mean expression of the chimeric protein in the cell line used in this study was $1.35 \times \cdot 10^5$ as determined by flow cytometry using a QiFIT DAKO kit and the monoclonal antibody 528 specific for the EGFR.

Synthesis of Atto390-CoA

Synthesis was carried out as described by Vivero-Pol et al. (13) by reaction of Atto390 maleimide (Atto-Tec GmbH) with the cysteine of CoA and purification by reverse-phase HPLC C_{18} chromatography.

Labeling of Cell Surface Expressed ACP–EGFR with Atto390 and of the Cellular Membrane with NR12S

Cells expressing the ACP–EGFR were cultured in 35-mm microdishes (Ibidi GmbH, cat. no. 81156) in DMEM (Life Technologies) supplemented with 10% fetal calf serum. Before measurements, the cells were brought into the resting state by serum starvation for at least 4 h. Enzymatic labeling of the ACP–EGFR on the plasma membrane was carried out in the dark for 10–20 min at room temperature in Tyrode's buffer supplemented with 10 mM $MgCl_2$ by the Sfp PPTase from *Bacillus subtilis* and the substrate, 2 μM Atto390-CoA. Cells were washed several times with Tyrode's buffer. For determination of Förster resonance energy transfer (FRET), cells were labeled for an additional 5 min with the membrane probe NR12S (14) serving as the FRET acceptor, using a $\geq$500-fold fresh dilution of the dye from a DMSO stock solution. The dishes were filled with Tyrode's buffer supplemented with 2 mM glucose and 5 mg/ml BSA and inverted on the upright microscope stage, such that the 60× objective directly faced the chamber membrane surface with the adherent cells. Experiments were conducted at room temperature. For experiments on activated EGFR, the cells were incubated for 30 min before receptor labeling with 2 μM of the EGFR-specific kinase inhibitor PD153035 (Calbiochem). The inhibitor was present throughout the process of dye labeling and subsequent measurement. The human-

recombinant EGF (Peprotech) was added to a concentration of 36 nM 3 min before the initiation of the measurements.

TCSPC Lifetime Image Acquisition

The excitation source was a multiphoton Ti:Sapphire fs laser (Chameleon Ultra, Coherent) tuned to 740 nm and pulsed at 80 MHz. Measurements were carried out on an upright Olympus scanning confocal microscope (Fluoview 1000) using a 60× 1.35 NA UPlanSApo oil immersion objective. The fluorescence signal at 480 nm (20 nm HW) was acquired with a SPAD detector (Micro Photon Devices), using the PicoHarp 300 TCSPC acquisition system of PicoQuant GmbH. Images were acquired with a scan speed of 20 μs/pixel at 256 × 256 pixel (x, y) resolution and 16-ps time resolution.

Lifetime Image Analysis

Analysis software was developed in *Mathematica* versions 7/8/9 (Wolfram Research). The program (ReadPicoQuant_bin.nb) reads and interprets bin files generated by the PicoQuant SymPhoTime program. The instrument response function (IRF) was obtained from the second harmonic-generated signals of KH_2PO_4 microcrystals excited at 960 nm and detected in the 480 nm (20 HW) emission window. Pixel signals were sorted according to intensity, and a mean response, computed from the top 392 levels, was fit to a seven-parameter (plus time) analytical function (*pulse*) consisting of a Gaussian distribution function plus an integrated Gaussian distribution function times an exponential decay (see Fig. 3B and Supporting Information).

In the case of the fluorescence images, an ROI was defined delineating the membrane, and the signals from the sorted pixels were fit to one- or two exponential decays, each component of which was characterized by an amplitude (counts) times a *signal* function, the convolution of the analytical IRF function with a normalized exponential decay [Eq. (1), Supporting Information]. The only free parameters in *signal* are the lifetime τ and a corresponding amplitude, all other parameters being derived from the IRF analysis. The advantage of *signal* is that it eliminates noise originating from deconvolution with an experimental IRF and fits the entire (ascending as well as descending) fluorescence time course. Despite the very asymmetric forcing function (IRF) of the TCSPC system, *signal* yields reproducible two-component analyses, even in the presence of short lifetime components that render tail-fitting routines unfeasible.

$$
\begin{aligned}
signal\left[\tau_{-}, t_{-}\right] : \quad &= a \cdot \frac{1}{2} Exp\left[\frac{\sigma^2 - 2\tau(t-t_0)}{2\tau^2}\right]\left(Erf\left[\frac{\sigma^2 + t_0\tau}{\sqrt{2}\sigma\tau}\right] + Erf\left[\frac{-\sigma^2 + (t-t_0)\tau}{\sqrt{2}\sigma\tau}\right]\right) \\
&- b \cdot \frac{\tau}{2(\tau-\omega)}\left(\begin{array}{l} Exp\left[-\frac{t-t_1}{\omega}\right]\left(Erf\left[\frac{t-t_1}{\sqrt{2\sigma_1}}\right] + Erf\left[\frac{t_1}{\sqrt{2\sigma_1}}\right]\right) - Exp\left[\frac{\sigma_1^2(\tau-\omega)^2 - 2(t-t_1)\tau\omega^2}{2\tau^2\omega^2}\right] \cdot \\ \left(Erf\left[\frac{\sigma_1^2(\tau-\omega) - (t-t_1)\tau\omega}{\sqrt{2}\sigma_1\tau\omega}\right] + Erf\left[\frac{t_1\tau\omega - \sigma_1^2(\tau-\omega)}{\sqrt{2}\sigma_1\tau\omega}\right]\right) \end{array}\right)
\end{aligned}
\tag{1}
$$

Because of the noise content, single pixel decays could only be fit with a single component (see example in Fig. 3C). In the case of the more precise two-component analyses of pixel data ordered and binned into groups (generally five, each with 100–1500 members) according to peak signal magnitude (see examples in Figs. 3D and 3E), a correction was applied to compensate for the data wraparound introduced by the 80 MHz repetition frequency. This procedure was implemented by adding to each given component the same component mirrored to a $t+1$ period (12.5 ns). In most cases, temporal channels were merged (generally by a factor of 5×), providing a major calculation speedup with no significant change in fit parameters. The derived amplitudes and lifetimes were subjected to examination and interpretation based on the corresponding images and two-dimensional histograms.

FRET Formalism

We assume that the donor–acceptor relationship applicable to the system under study corresponds reasonably to the treatment of Bastiaens et al. (22) of a single donor separated by a given distance (along the normal), r_{Dm} (subscript: donor-membrane), from a plane of acceptors with surface density σ. In the form expressed in Eq. (2), the index i denotes the different experimental conditions and molecular configurations that can be adopted, $k_{t,i}$ is the rate constant for energy transfer, c_0 is a constant (21), E_i is the FRET efficiency, τ_o is the fluorescence lifetime of the donor in the absence of the acceptor, and the Förster transfer distance R_o is defined in terms of the canonical (rapid rotational redistribution) value (2/3) for the orientation factor κ^2. The latter assumption introduces little error in the estimations of distances, particularly in the relative values [Eq. (3)], in the event that at least one partner is mobile (22). The estimated R_o for the Atto390-NR12S pair is 5.4 nm (Fig. 3A). We favor the FRET expression in terms of the transfer rate rather than the transfer efficiency E because of its more direct functional relationship to the quantities of greatest interest in this study, r_{Dm} and σ (21). Noteworthy is the inverse fourth-order dependence of the transfer rate constant on distance as opposed to the sixth-order dependence for an isolated donor–acceptor pair; k_t is also proportional to

σ, the acceptor density in the plasma membrane, for which the assumption of a uniform planar disposition is a reasonable simplification. For example, the effect of plasma membrane curvature on FRET has been shown to be negligible (23).

$$k_{t,i}\tau_0 = \frac{E_i}{1-E_i} = \frac{\tau_0}{\tau_i} - 1 = \frac{\pi}{2} R_o^6 \left(\frac{\sigma}{r_{Dm,i}^4} \right) \qquad (2)$$

$$R_o^6 = c_0 J n^{-4} \kappa^2 Q_{D,0}$$

Results

Molecular Modeling of the Atto390 Fluorophore Covalently Coupled to the Acyl Carrier Protein–EGFR Ectodomain in the Self-Inhibited and in the Liganded Conformations

Molecular model building was performed by combining the coordinates from the PDB structures 3NJP (17) of the EGFR liganded extracellular receptor domains (I–IV), 1NQL (3) of the EGFR unliganded extracellular receptor domains (I–IV), and the NMR coordinates from the PDB structure 1ACP (24) for the ACP motif. In the chimeric protein, the latter is attached to the amino terminal amino acid (shown as blue spheres in the diagrams) of the full-length EGFR sequence. According to the structures optimized using GROMACS 4.55 (19) (Figs. 2A and 2B), the Atto390 fluorophore (Fig. 3A) attached to serine 36 in the ACP motif would be located ~60 and ~120 Å, respectively, from the C terminus of domain IV (shown as gold spheres), which connects to the transmembrane segment and cytoplasmic domains (not shown) in both the presumptive unliganded and liganded states. The depicted structures are snapshots of an ensemble of possible conformations of the attached tag. Exact distance estimations are not feasible, because rather short 10 ns MD simulations were carried out. However, the approximate twofold difference in the

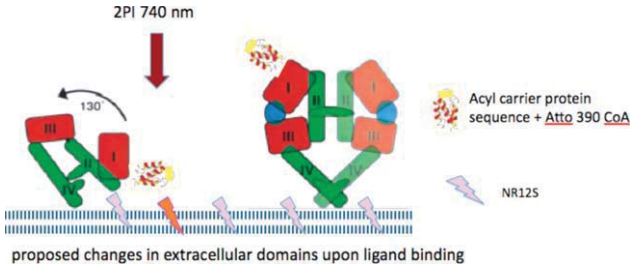

Figure 1. Schematic of the experimental design. Stick representations of full-length EGFR in the unliganded and inhibited conformation (left) and liganded dimer (right); adapted from illustrations in Ferguson (15). The blue box on the ACP tag attached to domain I denotes Atto390. The "thunderbolts" in the cell membrane denote the acceptor NR12S. The downward arrow denotes the 740 nm two-photon laser excitation pulse. The Atto390 on the left shows quenching (lighter blue) due to resonance energy transfer to the nearest NR12S acceptor that shows increased fluorescence (red) compared with the Atto390 on the right.

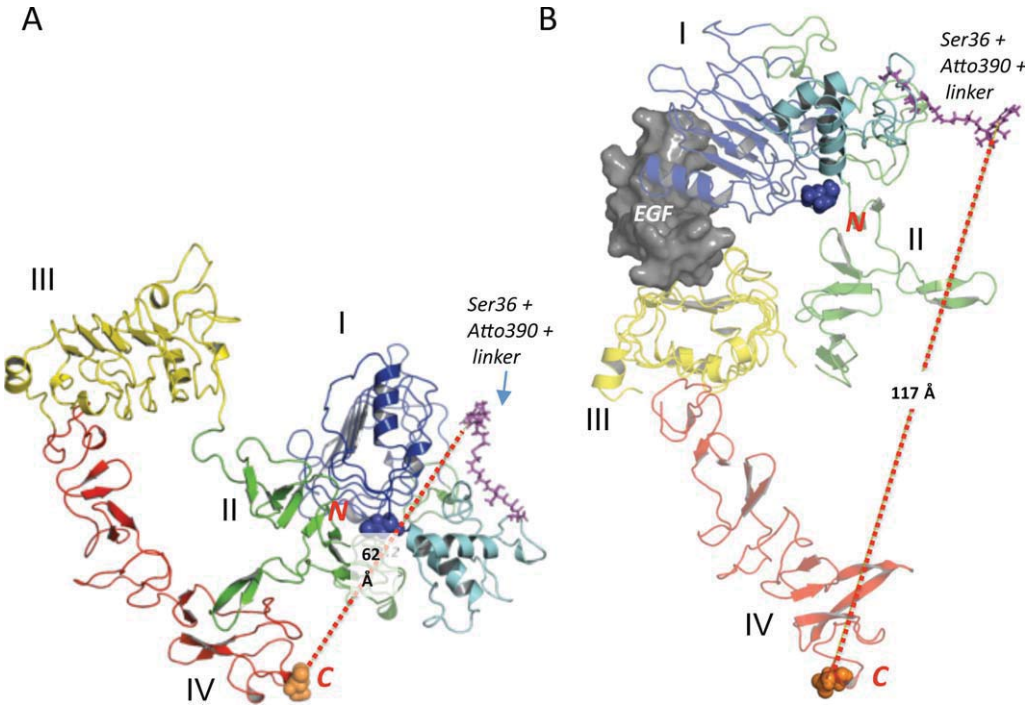

Figure 2. Molecular dynamics estimations of the distance of the Atto390-ACP-tagged EGFR to the C-terminus of domain IV in the unactivated, inhibited, and EGF ligand-bound conformations. **A:** Model of the structure of the ectodomain of the self-inhibited, resting, chimeric ACP-EGFR (1NQL) (3) with Atto390 attached covalently to serine 36 of the ACP moiety, showing its calculated distance to the C-terminus of domain IV after energy minimization and MD simulation. ACP, cyan; domain I 1–165, blue; domain II 166–309, green; domain III 310–481, yellow; domain IV 482–614, red with C-terminus orange. **B:** Model of the structure of the ectodomain of the extended, ligand-bound, chimeric ACP-EGFR (3NJP) (17) with Atto390 attached covalently to serine 36 of the ACP moiety, showing its calculated distance to the C-terminus of domain IV after energy minimization and MD simulation. Same color coding as in A.

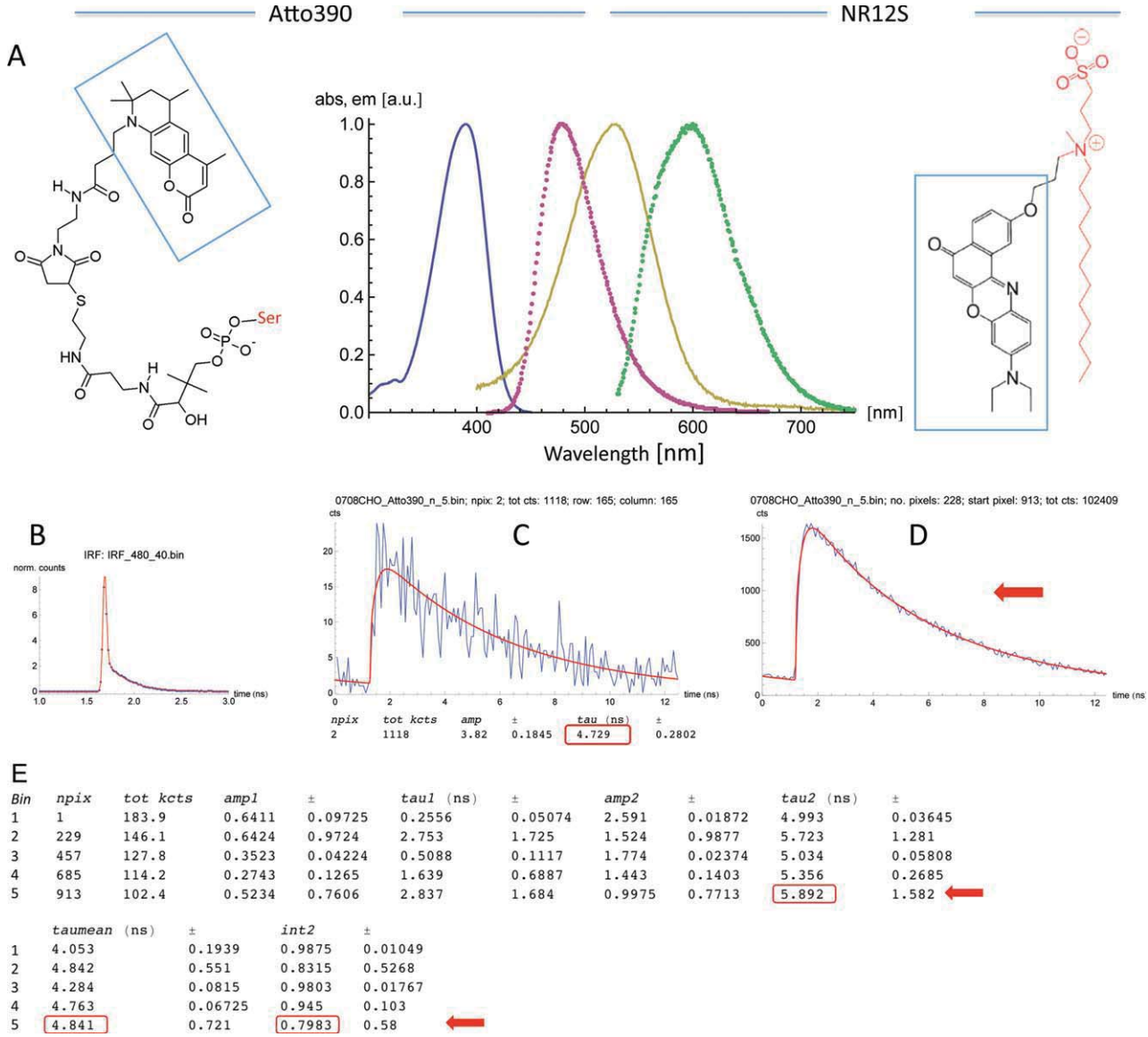

Figure 3. FRET donor and acceptor spectra and lifetime analysis. **A:** Donor and acceptor chemical structures and normalized excitation spectra (solid lines) and emission spectra (discontinuous lines). The fluorophore moieties are enclosed by blue rectangles. The calculation of R_o was performed (21) with the following parameters: c_o, $8.8 \cdot \times 10^{-28}$; J, $1.54 \cdot \times 10^{32}$; n, 1.333; κ^2, 2/3; and $Q_{D,o}$, 0.9 (manufacturer's data). **B:** Instrument response function (IRF). Second harmonic signal from KH_2PO_4 microcrystals; blue, data points; red, fitted function. **C:** TCSPC trace for the single pixel 2 (npix2) in the intensity collected data for this file in blue with superposition of a single component fit in red. **D:** TCSPC trace (blue) and two-component fit (red) for the lowest of the five intensity bins of the pixel values (see the full analysis information for this bin designated with the red arrows in E). **E:** Table of fit parameters for the five bins. See text for details. Errors are standard errors of the mean values (SEM), propagated according to the respective parameters.

distance of the dye molecule to the outer leaflet of the membrane, where the NR12S dye is located, would be expected to result in a large difference in the donor lifetime because of the fourth power distance dependence of FRET [Eq. (2)].

Labeling of the Chimeric ACP–EGFR with Donor Atto390 and the External Leaflet of the Cellular Membrane with Acceptor NR12S

The ACP–EGFR protein was expressed well in mammalian cells and inserted into the extracellular membrane. It exhibited the properties of wild-type EGFR; that is, the receptor bound EGF and was transphosphorylated as well as showing the kinetics of downstream signaling and endocytosis characteristic of native EGFR (see Supporting Information Figs. S1 and S2). Labeling of the ACP tag by the donor fluorophore Atto390-CoA by Sfp PPTase proceeded as described in the Materials and Methods section.

Lipid soluble fluorescence dyes can be used to externally label the plasma membranes, but most exhibit rapid flip-flop between the outer and inner leaflets and are internalized rapidly, distributing to all intracellular membrane compartments. Recently, Kucherak et al. (14) described a derivative of Nile Red, NR12S, conjugated with a zwitterionic group and a long

hydrophobic chain (Fig. 3A). This compound selectively stains the outer leaflet of lipid bilayers and exhibits negligible flip-flop, leading to exceptionally long retention time at plasma membranes of mammalian cells (14,25). The spectral properties of NR12S incorporated into lipid bilayers are complex, with solvatochromic shifts in both absorption and emission as a function of lipid composition and order (14). In the cellular context, the absorption spectrum has a peak in the 525–530 nm range and the fluorescence spectrum at 585–605 nm. NR12S was selected as a good FRET acceptor match for the Atto390 donor fluorophore attached to EGFR (see below). Atto390 exhibits a large Stokes shift, such that its excitation maximum (390 nm) lies at a minimum in NR12S absorption while its emission (peak at 479 nm) has a good overlap with the absorption spectrum of NR12S in lipid membranes with a calculated R_o of 5.4 nm (Fig. 3A).

TCSPC Lifetime Measurements of FRET in Living Mammalian Cells

Images of cells labeled with the Atto390 donor in the absence or presence of the NR12S acceptor showed a strong 480 ± 20 nm signal localized to the plasma membrane upon two-photon excitation at 740 nm. FRET occurring in the presence of the NR12S acceptor was assessed by the reduction of the donor lifetime (26), because the large excess of acceptor emission excited directly in all regions of the plasma membrane precluded methods based on sensitized emission. Image pixels were sorted by intensity and subjected to a single component decay analysis, yielding lifetimes of 4.6 ± 0.3 ns for the top 100 intensity values under all conditions (Fig. 3C). Cells lacking the Atto390 label exhibited low-level background signals originating from generalized intracellular locations and with lifetime fits of <1 ns. This component is primarily attributable to NADH (27) and was minimized by applying a mask restricting the analyzed pixels primarily to the plasma membrane. The mask was double-sided and could also be used to limit the intensity selection to any arbitrary region, for example, so as to exclude the highest values. Spatial binning was not used in order to minimize the influence of ambiguous edge pixels.

After binning the foreground pixels into groups of 100–1500, it was possible to perform reproducible lifetime determinations using the formalism accounting for two components as well as the perturbation arising from the short measurement period of 12.5 ns [Eq. (1) and Fig. 3D]. The analysis program provided statistical measures for all the fit parameters [two amplitudes, two lifetimes, two intensities (relative amplitude $\times$ lifetime), and mean (amplitude-weighed) lifetime] (Fig. 3E), from which two-dimensional histograms and images showing the spatial distribution of the computed lifetimes were generated (see examples in Figs. 4–7 and Table 1). The fluorescence decay of the Atto390 probe was perceived as a single major component (τ_2) of >5 ns accounting for 87–98% of the signal intensity, and the presence of FRET was manifested by changes in τ_2. The lifetime of the donor reproduces that supplied by the manufacturer as well as our own determinations in another study of Atto390 attached to nucleic acids, which yielded values of 6.0 and 1.6 ns (93% and 7% intensity, respectively). Neither the single component fits, as indicated earlier, nor the amplitude-weighted mean lifetimes derived from two-component fits, generally used as a FRET measure in imaging applications, were useful due to the presence of the variable shorter $\sim$1 ns (τ_1) component unaffected appreciably by FRET.

Measurements on Starved Cells

Figure 4 features images from different experiments of three cells labeled with the donor Atto390. The color-coded images are of the total intensity, the intensity processed with a binary mask, and the corresponding determinations of τ_2 obtained by binning the pixels into five groups and fitting by two-component analysis. The global mean $\pm$ SEM of τ_2 from these and other data ($n = 9$ images, each of 1–2 cells, with 500–7500 analyzed pixels) was 5.26 ± 0.06 ns (see Table 1 and Fig. 7). The distribution of lifetimes in any given cell was fairly narrow and lacked an apparent correlation with intensity. Measurement of the donor in the presence of the kinase inhibitor PD153035 without added acceptor also yielded similar lifetimes (Table 1). In a limited set of measurements, fixation of the Atto390-labeled cells (3.7% PFA, 10–15 min at room temperature) was shown not to have had a discernible effect on the lifetimes.

Quiescent Atto390-labeled living cells were exposed to increasing concentrations (0.2–1 μM) of the NR12S acceptor probe. A systematic and consistent diminution of τ_2 was observed (Table 1, Fig. 7). It was determined that 0.5 and 1 μM NR12S led to equivalent values, and therefore, the majority of experiments were conducted with 0.5 μM acceptor. The global mean $\pm$ SEM of τ_2 was 4.81 ± 0.03 ns ($n = 15$), corresponding to a decrease of 9%. Images of signals from cells with donor plus 0.5 μM acceptor and the calculated τ_2 lifetime are shown in Figure 5. The τ_2 values for 0.2 and 1 μM NR12S were 4.97 ± 0.05 ns ($n = 3$) and 4.81 ± 0.01 ns ($n = 2$), respectively (Fig. 7). Equation (2) predicts a linear dependency of the transfer rate on acceptor density. A more detailed assessment (additional acceptor concentrations) was not feasible in the context of these experiments. Furthermore, elucidation of the relationship between membrane loading and external dye concentration, the dependence on incubation conditions, and of the uniformity of probe distribution and properties, particularly in the vicinity of the receptor, would constitute a separate investigation.

Measurements After Addition of EGF

The ligand EGF was added in the presence of a specific EGFR kinase inhibitor PD153035. The latter does not affect EGF binding but prevents endocytosis, thereby retaining the receptor in its plasma membrane environment. Addition of saturating concentrations of EGF increased the donor lifetime to τ_2 values (5.10 ± 0.03, $n = 12$), close to those obtained in the absence of acceptor (3.0% lower). Images of some of these cells are shown in Figure 6.

Interpretation of the FRET Data in Terms of Distances

The results of several sets of experiments conducted under the various conditions are presented in Table 1 and Figure 7. The

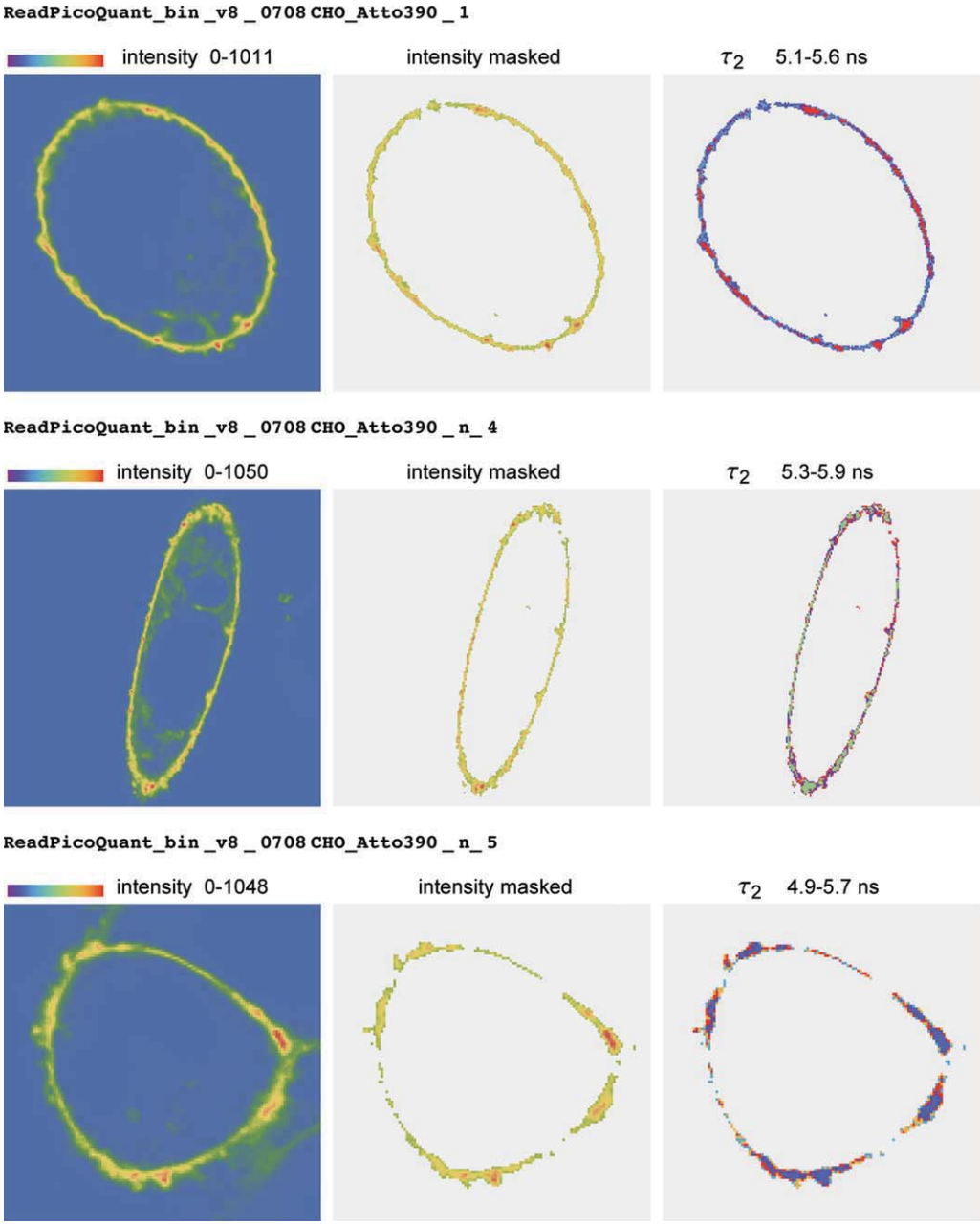

Figure 4. Gallery of images of cells labeled only with donor, Atto390-ACP-EGFR. Left, intensity images of the donor emission in the selected ROI; middle, masked intensity image; right, τ_2 values corresponding to the masked pixels. The LUT at the left applies to the rescaled peak intensity for the left and middle images and for the given range of lifetime values (right image).

data show a consistently shorter donor lifetime for the starved cells in the presence of acceptor than those measured after binding EGF. One can use Eq. (2) in two ways to estimate consistency with the distance estimations from the molecular modeling (Fig. 2). We first apply the equation to each condition of interest (*a*: donor; *b*: donor + acceptor; *c*: donor + acceptor + EGF) and evaluate the following relationship, in which common parameters (R_o^6, σ) conveniently cancel in the ratio.

$$\frac{r_{Dm,c}}{r_{Dm,b}} = \left(\frac{\tau_{2,a}/\tau_{2,b} - 1}{\tau_{2,a}/\tau_{2,c} - 1}\right)^{1/4} \quad (3)$$

Introduction of the respective values of the liganded and unliganded forms of the EGFR into Eq. (3) yielded a value of 1.3 ± 0.2 (SEM), which can be compared to the (single) estimation of $11.2/6.2 = 1.8$ from molecular modeling (Fig. 1). The agreement is not unreasonable in view of the conceptual and experimental uncertainties associated with these measurements and simulations. Thus, the value of 1.8 would be reduced to 1.5–1.7 by adding the finite distance between the C-terminus of domain IV and the NR12S probe inserted into the outer leaflet of the plasma membrane to both the

numerator and denominator of the molecular modeling ratio; we estimate this contribution as ~1–3 nm (28).

A second application of Eq. (2) is in the comparison of the most reliable FRET data of condition *b* with those obtained under condition *c* at the same acceptor concentration. A range of $r_{Dm,b}$ 6.0–6.4 nm was calculated by using the mean τ_2 values and specifying an acceptor density σ of 0.003–0.004 probe molecules/nm^2. The same range of σ, applied to condition *c*, that is, after addition of EGF, would correspond to an $r_{Dm,c}$ of >7.8 nm. Reliable quantitative determinations of membrane probes applied externally to cells are not available in the literature. One study using bulk probe concentrations of 0.2–7.5 μM yielded estimates for σ of 0.001–0.01 (29), values consistent with our calculations. Table 1 also provides an estimate of the transfer rate and energy transfer efficiencies.

The above methods of analysis provide convincing evidence for a significant extension of the EGFR after addition of EGF, such that the distance of the N-terminus from the membrane increases, in conformity with the model featured in Figures 1 and 2.

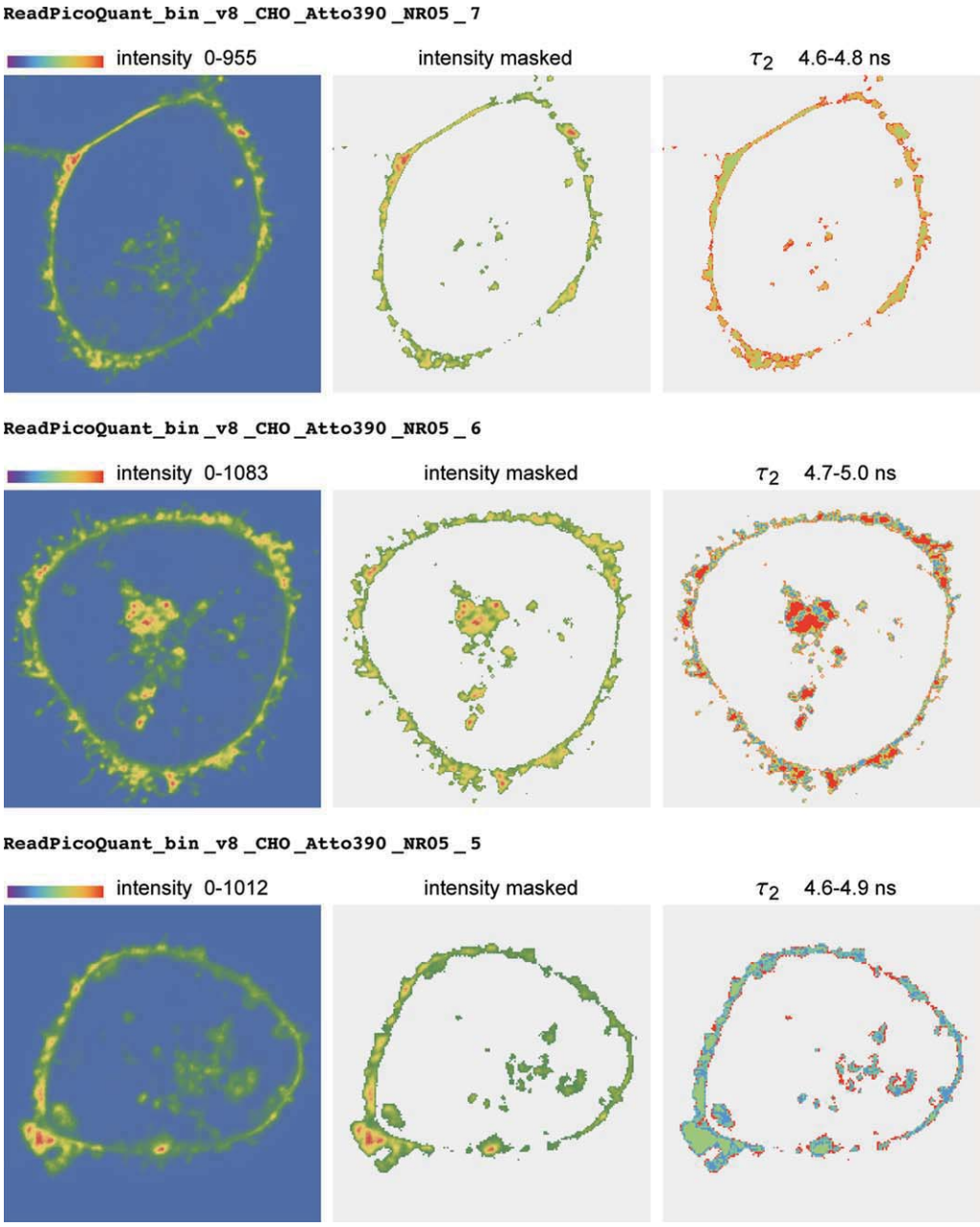

Figure 5. Gallery of images of cells labeled with donor and acceptor (0.5 μM NR12S). Details as in Figure 4.

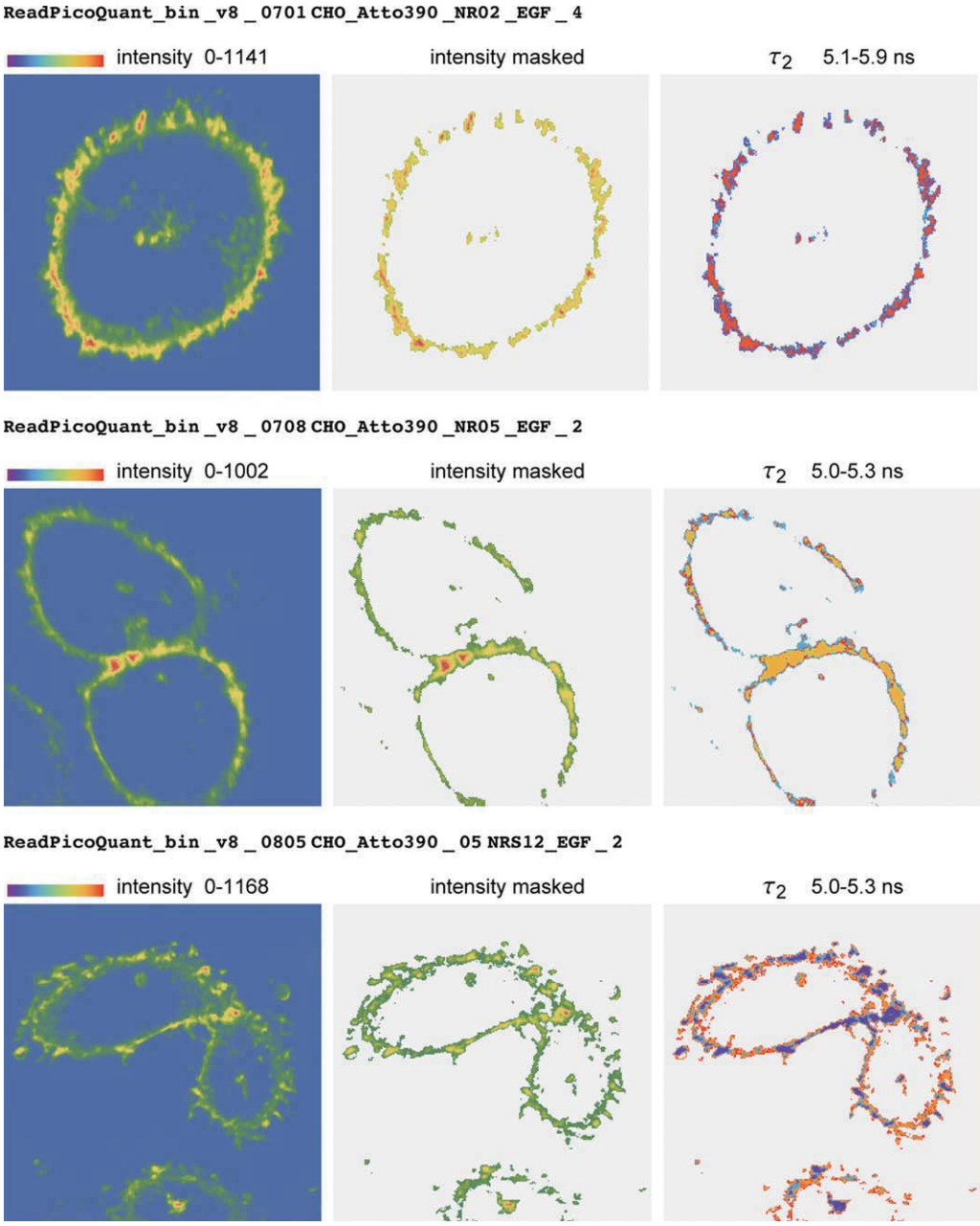

Figure 6. Gallery of images of cells labeled with donor and acceptor (0.5 μM NR12S) in the presence of EGF and kinase inhibitor PD153035. Details as in Figure 4.

Discussion

The FRET–FLIM determinations demonstrate that the N-terminus of the unliganded EGFR in the quiescent living cell is situated much closer to the membrane than after EGF addition. This result supports the model according to which the inactive receptor in quiescent cells is predominantly in the self-inhibited configuration (7,9,30) shown in Figure 2A. Starving the cells as well as measurements at room temperature favor the quiescent structure. In contrast, the X-ray crystallographic structure of the liganded EGFR features monomers extended and dimerized in a back-to-back configuration (1,2), such that the distance of the amino terminus from the cell membrane (Fig. 2B) would be approximately double. The molecular modeling is compatible with these interpretations in that it predicts that the extended liganded EGFR dimer would have a distance of the ACP–EGFR domain I to the cell membrane considerably greater than the R_0 for the Atto 390-NR12S donor–acceptor pair of 5.4 nm and should thus show little energy transfer, whereas the inhibited structure would bring the dye pair close to the Förster transfer distance.

Table 1. Lifetime analyses and FRET calculations

SAMPLE	[NR12S] (μM)	τ_2(ns)	$10^{-7} \cdot k_t(s^{-1})$	E
Atto390-ACP-EGFR	0	5.26 ± 0.06		–
	0.2	4.97 ± 0.05		0.06 ± 0.01
	0.5	4.81 ± 0.03	1.8±1.1	0.09 ± 0.01
	1.0	4.81 ± 0.01		0.09 ± 0.01
Atto390-ACP-EGFR + EGF + PD	0.2	5.22 ± 0.04		–
	0.5	5.10 ± 0.03		0.03 ± 0.01
Atto390-ACP-EGFR + PD	0	5.17 ± 0.12		

Error: standard error of the mean (SEM). For other definitions, see Eq. (1).

Our quantitative treatment of the FRET–FLIM data was based on a formalism applicable to transfer from a donor probe located in the ectodomain of a transmembrane protein to an array of acceptor probes integrated into the supporting lipid bilayer (22).

The structures shown in Figure 2 are snapshots of the presumed configurations adopted by the EGFR in the living cell, inasmuch as the MD simulations were initiated from the X-ray self-inhibited or liganded species, respectively. Although the interdomain contacts of domains II and IV of the self-inhibited structure remained and the molecule did not extend during the MD simulations, we assume that in living cells, there exists flexibility in both structures, including a "breathing" of the inhibited form. As mentioned earlier, the actual distance between the donor and acceptor is probably larger than that calculated from the molecular modeling, because a seven amino acid linker connects the C-terminus of domain IV to the transmembrane segment (17) and the acceptor dye moiety is presumably immersed in the membrane. Using the original diffraction data set of Ogiso et al. (2), Lu et al. (17) calculated a refined annealing-composite omit map to determine the position of domain IV in the liganded dimer. The structure of domain IV could be superposed by bending and displacing the C-termini by 10 Å from the monomer (3) to dimer structures (17). Disulfide crosslinking studies of cells expressing single cysteine replacements established that the seven amino acid linker between the C terminus (residue 614) of domain IV, and the transmembrane segment is highly flexible but has no preferential pairing upon EGF binding (17). Similar disulfide crosslinking with substitutions of the amino acids in the 23-residue transmembrane segment, however, exhibited a strong peak at residue 624 and a weaker one at 627 only upon EGF binding, indicating an association of the transmembrane domains of the dimer only in the first two α-helical turns.

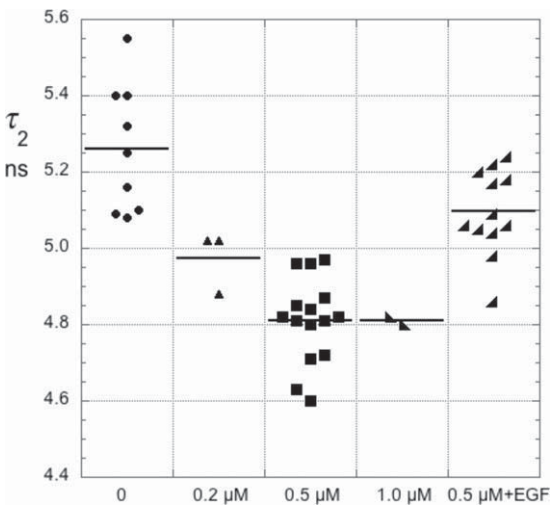

Figure 7. Fluorescence lifetimes (τ_2) from four independent experiments and different conditions. The abscissa denotes the different experimental conditions: the concentration of acceptor present and the presence of EGF where applicable. The mean τ_2 values are indicated by horizontal lines for each condition. See text for details.

The fact that the linker region is flexible allows other orientations of EGFR, such that inactive, unliganded dimers might form as proposed by Jura et al. (31), or asymmetric dimers might form as seen with the invertebrate *Drosophila* EGFR (32). The latter viewpoint has been championed by the group of Martin-Fernandez (33–35), which has focused on biophysical measurements to elucidate the structure of the "high-affinity" EGFR implicated by Scatchard EGF-binding plots showing upward curvature (negative cooperativity) at very low-EGF concentrations. This group has presented evidence from FRET/FLIM measurements with a labeled EGF ligand (<1 nM) as donor and a membrane carbocyanine dye as acceptor for the existence of a small cohort (10–15%) of "high-affinity" dimers, which would be asymmetric and lie on (parallel to) the cell membrane. Unfortunately, the use of EGF as the donor instead of a label attached to the receptor as in the present study, does not permit a useful comparison of the inhibited monomer conformation from the extended dimer configurations inasmuch as EGF interacts with the open domain III in the inhibited conformation and is thus situated at a similar distance from the membrane in both forms. Our measurements, performed exclusively with saturating concentrations of EGF, gave no indication of a substantial contribution from a structure of the liganded receptor with the N-terminus situated close to the membrane.

A previous publication reported little FRET between an amino terminal fused YFP–EGFR chimera and concluded that the EGFR receptor in the cell membrane exists in an extended form and probably as a constitutive dimer (11). This transgene, however, shows spontaneous activation of the receptor

in the absence of EGF, a phenomenon that does not occur in starved cells expressing wild-type receptor, suggesting that the YFP-chimera may have been dimerizing via the YFP moiety and not adopting the normal configuration of the normal receptor in the membrane. It is well known that YFP without the A206K mutation undergoes spontaneous dimerization (36). However, this mutation was not used in the Kozer et al. (11) study. In addition, the Rh-DHPE (LissamineTM rhodamine B 1,2-dihexadecanoyl-sn-glycero-3-phospho-ethanolamine) acceptor used by these authors was not restricted to the outer leaflet of the cell membrane. Finally, Kozer et al. (11) used a hematopoietic cell-line BaF/3 for their biophysical studies. Although this cell line lacks endogenous ErbB proteins, it is a very different than the epithelial cells that normally express the ErbB family. We assume that both the cell type and the large-added protein domain led to significant changes in the disposition of the EGFR ectodomain compared to other cells expressing EGFR. Only the studies of such hematopoietic cell lines have led to reports of a large fraction of dimers of EGFR in resting cells with expression levels of 50,000 receptors and of signaling being initiated from tetramers (37). In contrast, studies of CHO and HeLa cell lines have shown predominantly monomeric EGFR receptors in cells expressing <100,000 receptors by a variety of measurements including fluorescence correlation spectroscopy (FCS) (38), number and brightness (N&B) (39), and single particle tracking (SPT) (40). Unliganded dimer formation is <30% even in cells with receptor numbers of 5×10^5 (39). SPT measurements have demonstrated similar diffusion constants of unliganded and liganded receptors even in A431 cells with 2×10^6 receptors, ruling out a predominance of preformed dimers and tetramers as preferential signaling platforms. As we discuss below, both the lipid composition of the BaF/3 cells and the promotion of dimer formation by YFP interactions probably account for the failure of Kozer et al. (11) to detect the inhibited conformation.

Assuming that the receptor is in a dynamic equilibrium between the extended (dimeric) and inhibited conformations, interactions preferential for one or the other conformation will perturb the fractional distribution. The high-lateral mobility of the EGFR, for example, determined by Lidke et al. (41), by FRAP, will contribute to population redistribution. From N&B determinations, Nagy et al. (39) inferred a greater fractional population of unliganded dimers in cells expressing 500,000 receptors than in those with 50,000 receptors, and Chung et al. (42) observed more dimers in cells with high-receptor densities using SPT. Saffarain et al. (38) showed by FCS that depletion of cholesterol from cells increased the number of unliganded dimers in living cells. Recent studies have also revealed that certain lipids have a profound effect on EGFR structure and activation (43). EGFR binds seven peptide growth factors, which elicit distinct physiological responses (44). It is possible that the conformational rearrangements induced by these natural ligands are somewhat different than those induced by EGF, suggesting that studies of these complexes in living cells by FRET–FLIM measurements may be informative.

The Bastiaens group has studied the key role of phosphatases in the deactivation of spontaneous signaling by EGFR from the plasma membrane (45,46). Their data suggest that spontaneous dimer formation can lead easily to transphosphorylation, constituting an activation mechanism operating in the absence of ligand. EGFR is overexpressed or mutated in many cancers, leading to increased activation and consequent unhindered growth (47,48). A more striking example of the importance of the self-inhibitory structure is the constitutively activated mutant EGFRvIII found in many gliomas (49,50), which has a deletion of residues 6–273 that eliminates parts of domains I and II. This mutant receptor cannot adopt the inhibited structure and thus may allow the transmembrane and kinase domains to more easily assume their activated conformations. It is important that the majority of the EGFR in normal epithelial cells be maintained in the inhibited state and that spontaneous dimer formation be controlled so as to restrain aberrant activation of the cell cycle and proliferation. Our data support the model of the quiescent monomer receptor in which part of the inhibition to self-activation is provided by a conformation of the receptor that features interaction of domain II with domain IV and brings domain I close to albeit not directly at the cell membrane.

During the revision of this report, a study appeared featuring extensive modeling by MD of various forms of the EGFR in a membrane environment (51). The authors concluded that the ectodomains of the monomeric and unliganded dimeric forms are intimately associated with the membrane, with only the active (liganded) dimer in an extended ("upright") configuration. Our data and conclusions do not support such a view, emphasizing the importance of as yet not fully understood structural and microenvironmental features of these complex molecules located in their native cellular milieu.

Acknowledgments

I.Z. was a student of the Faculty of Biology of the Adam Mickiewicz University, Poznan, Poland, supported by an Erasmus EU exchange fellowship with the Georg-August-University of Göttingen. A.L. was supported by the German Federal Ministry of Education and Research (BMBF). The authors thank F. Wouters for providing the multiphoton laser system. D.J.A-J. and T.M.J. conceived of the experiments; C.F and D.J.A-J. made the EGFR constructs and isolated the cell lines; D.J.A-J. synthesized and purified the Atto390 CoA compound; I.Z and A.L. performed the measurements; R.K. performed the model building; A.S.K. provided the NR12S; G.B. helped with the alignment of the laser and guided the TCSPC measurements; T.M.J. developed the analysis software and analyzed the data; D.J.A-J. and T.M.J. wrote the manuscript. The authors declare no conflict of interest.

Literature Cited

1. Garrett TPJ, McKern NM, Lou MZ, Elleman TC, Adams TE, Lovrecz GO, Zhu HJ, Walker F, Frenkel MJ, Hoyne PA, et al. Crystal structure of a truncated epidermal growth factor receptor extracellular domain bound to transforming growth factor α. Cell 2002;110:763–773.

2. Ogiso H, Ishitani R, Nureki O, Fukai S, Yamanaka M, Kim JH, Saito K, Sakamoto A, Inoue M, Shirouzu M, et al. Crystal structure of the complex of human epidermal growth factor and receptor extracellular domains. Cell 2002;110:775–787.
3. Ferguson KM, Berger MB, Mendrola JM, Cho HS, Leahy DJ, Lemmon MA. EGF activates its receptor by removing interactions that autoinhibit ectodomain dimerization. Mol Cell 2003;11:507–517.
4. Lemmon MA, Bu ZM, Ladbury JE, Zhou M, Pinchasi D, Lax I, Engelman DM, Schlessinger J. Two EGF molecules contribute additively to stabilization of the EGFR dimer. EMBO J 1997;16:281–294.
5. Garrett TPJ, McKern NM, Lou MZ, Elleman TC, Adams TE, Lovrecz GO, Kofler M, Jorissen RN, Nice EC, Burgess AW, et al. The crystal structure of a truncated ErbB2 ectodomain reveals an active conformation, poised to interact with other ErbB receptors. Mol Cell 2003;11:495–505.
6. Ozcan F, Klein P, Lemmon MA, Lax I, Schlessinger J. On the nature of low- and high-affinity EGF receptors on living cells. Proc Natl Acad Sci USA 2006;103:5735–5740.
7. Schmitz KR, Ferguson KM. Interaction of antibodies with ErbB receptor extracellular regions. Exp Cell Res 2009;315:659–670.
8. Li S, Schmitz KR, Jeffrey PD, Wiltzius JJ, Kussie P, Ferguson KM. Structural basis for inhibition of the epidermal growth factor receptor by cetuximab. Cancer Cell 2005;7: 301–311.
9. Schmiedel J, Blaukat A, Li S, Knochel T, Ferguson KM. Matuzumab binding to EGFR prevents the conformational rearrangement required for dimerization. Cancer Cell 2008;13:365–373.
10. Lemmon MA. Ligand-induced ErbB receptor dimerization. Exp Cell Res 2009;315: 638–648.
11. Kozer N, Henderson C, Jackson JT, Nice EC, Burgess AW, Clayton AH. Evidence for extended YFP-EGFR dimers in the absence of ligand on the surface of living cells. Phys Biol 2011;8:066002.
12. George N, Pick H, Vogel H, Johnsson N, Johnsson K. Specific labeling of cell surface proteins with chemically diverse compounds. J Am Chem Soc 2004;126:8896.
13. Vivero-Pol L, George N, Krumm H, Johnsson K, Johnsson N. Muticolor imaging of cell surface membrane proteins. J Am Chem Soc 2005;127:12770–12771.
14. Kucherak OA, Oncul S, Darwich Z, Yushchenko DA, Arntz Y, Didier P, Mely Y, Klymchenko AS. Switchable nile red-based probe for cholesterol and lipid order at the outer leaflet of biomembranes. J Am Chem Soc 2010;132:4907–4916..
15. Ferguson KM. Active and inactive conformations of the epidermal growth factor receptor. Biochem Soc Trans 2004;32:742–745.
16. The PyMOL Molecular Graphics System. 1.5.0.4: Schrödinger, LLC.
17. Lu C, Mi L, Grey M, Zhu J, Graef E, Yokoyama S, Springer T. Structural evidence for loose linkage between ligand binding and kinase activation in the epidermal growth factor receptor. Mol Cell Biol 2010;30:5432.
18. Ponder J, Case D. Force fields for protein simulations. Adv Prot Chem 2003;66:27–85.
19. Hess B, Kutzner C, van der Spoel D, Lindahl E. GROMACS 4: Algorithms for highly efficient, load-balanced, and scalable molecular simulation. J Chem Theory Comp 2008;4:435–447.
20. George N. A new method for protein labeling with small molecules based on acyl carrier protein. [Doc. Sci.]. Lausanne: École Polytechnique Fédérale de Lausanne; 2006. 149 p.
21. Jares-Erijman EA, Jovin TM. Imaging molecular interactions in living cells by FRET microscopy. Curr Opin Chem Biol 2006;10:1–8.
22. Bastiaens P, de Beus A, Lacker M, Somerharju P, Vauhkonen M, Eisinger J. Resonance energy transfer from a cylindrical distribution of donors to a plane of acceptors. Location of apo-B100 protein on the human low-density lipoprotein particle. Biophys J 1990;58:665–675.
23. Fung BK, Stryer L. Surface density determination in membranes by fluorescence energy transfer. Biochemistry 1978;17:5241–5248.
24. Kim Y, Prestegard J. Refinement of the NMR structures for acyl carrier protein with scalar coupling data. Proteins 1990;8:377.
25. Darwich Z, Klymchenko A, Kucherak O, Richert L, Mély Y. Detection of apoptosis through the lipid order of the outer plasma membrane leaflet. Biochem Biophys Acta-Biomembr 2012;1818:3049–3054.
26. Duncan RR, Bergmann A, Cousin MA, Apps DK, Shipston MJ. Multi-dimensional time-correlated single photon counting (TCSPC) fluorescence lifetime imaging microscopy (FLIM) to detect FRET in cells. J Microsc 2004;215:1–12.
27. Chia TH, Williamson A, Spencer DD, Levene MJ. Multiphoton fluorescence lifetime imaging of intrinsic fluorescence in human and rat brain tissue reveals spatially distinct NADH binding. Opt Expr 2008;16:4237–4249.
28. Bessman NJ, Lemmon MA. Finding the missing links in EGFR. Nat Struct Mol Biol 2012;19:1–3.
29. Sengupta P, Holowka D, Baird B. Fluorescence resonance energy transfer between lipid probes detects nanoscopic heterogeneity in the plasma membrane of live cells. Biophys J 2007;92:3564–3574.
30. Ferguson KM. Structure-based view of epidermal growth factor receptor regulation. Annu Rev Biophys 2008;37:353–373.
31. Jura N, Endres NF, Engel K, Deindl S, Das R, Lamers MH, Wemmer DE, Zhang X, Kuriyan J. Mechanism for activation of the EGF receptor catalytic domain by the juxtamembrane segment. Cell 2009;137:1293–1307.
32. Alvarado D, Klein DE, Lemmon MA. Structural basis for negative cooperativity in growth factor binding to an EGF receptor. Cell 2010;142:568–579.
33. Martin-Fernandez M, Clarke DT, Tobin MJ, Jones SV, Jones GR. Preformed oligomeric epidermal growth factor receptors undergo an ectodomain structure change during signaling. Biophys J 2002;82:2415–2427.
34. Roberts SK, Tynan CJ, Winn M, Martin-Fernandez ML. Investigating extracellular in situ EGFR structure and conformational changes using FRET microscopy. Biochem Soc Trans 2012;40:189–194.
35. Tynan CJ, Roberts SK, Rolfe DJ, Clarke DT, Loeffler HH, Kastner J, Winn MD, Parker PJ, Martin-Fernandez ML. Human epidermal growth factor receptor (EGFR) aligned on the plasma membrane adopts key features of Drosophila EGFR asymmetry. Mol Cell Biol 2011;31:2241–2252.
36. Zacharias DA, Violin JD, Newton AC, Tsien RY. Partitioning of lipid-modified monomeric GFPs into membrane microdomains of live cells. Science 2002;296:913–916.
37. Clayton AH, Walker F, Orchard SG, Henderson C, Fuchs D, Nice EC, Burgess AW. Ligand-induced dimer-tetramer transition during the activation of the cell surface epidermal growth factor receptor-A multidimensional microscopy analysis. J Biol Chem 2005;280:30392–30399.
38. Saffarian S, Li Y, Elson EL, Pike LJ. Oligomerization of the EGF receptor investigated by live cell fluorescence intensity distribution analysis. Biophys J 2007;93: 1021–1031.
39. Nagy P, Claus J, Jovin TM, Arndt-Jovin DJ. Distribution of resting and ligand-bound ErbB1 and ErbB2 receptor tyrosine kinases in living cells using Number and Brightness analysis. Proc Natl Acad Sci USA 2010;107:16524–16529.
40. Low-Nam ST, Lidke KA, Cutler PJ, Roovers RC, van Bergen en Henegouwen PMP, Wilson BS, Lidke DS. ErbB1 dimerization is promoted by domain co-confinement and stabilized by ligand binding. Nat Struct Mol Biol 2011;18: 1244–1249.
41. Lidke DS, Lidke KA, Rieger B, Jovin TM, Arndt-Jovin DJ. Reaching out for signals: Filopodia sense EGF and respond by directed retrograde transport of activated receptors. J Cell Biol 2005;170:619–626.
42. Chung I, Akita R, Vandlen R, Toomre D, Schlessinger J, Mellman I. Spatial control of EGF receptor activation by reversible dimerization on living cells. Nature 2010;464: 783–787.
43. Coskun U, Grzybek M, Drechsel D, Simons K. Regulation of human EGF receptor by lipids. Proc Natl Acad Sci USA 2011;108:9044–9048.
44. Schneider MR, Wolf E. The epidermal growth factor receptor ligands at a glance. J Cell Physiol 2009;218:460–466.
45. Offterdinger M, Bastiaens PI. Prolonged EGFR signaling by ERBB2-mediated sequestration at the plasma membrane. Traffic 2008;9:147–155.
46. Offterdinger M, Georget V, Girod A, Bastiaens PI. Imaging phosphorylation dynamics of the epidermal growth factor receptor. J Biol Chem 2004;279:36972–36981.
47. Arteaga CL. ERBB receptors in cancer: Signaling from the inside. Breast Cancer Res 2011;13:304.
48. Al Dayel F. EGFR mutation testing in non-small cell lung cancer (NSCLC). J Infect Publ Health 2012;5 (Suppl 1):S31–S34.
49. Huang PH, Mukasa A, Bonavia R, Flynn RA, Brewer ZE, Cavenee WK, Furnari FB, White FM. Quantitative analysis of EGFRvIII cellular signaling networks reveals a combinatorial therapeutic strategy for glioblastoma. Proc Natl Acad Sci USA 2007; 104:12867–12872.
50. Gan HK, Kaye AH, Luwor RB. The EGFRvIII variant in glioblastoma multiforme. J Clin Neurosci 2009;16:748–754.
51. Arkhipov A, Shan Y, Das R, Endres NF, Eastwood MP, Wemmer DE, Kuriyan J, Shaw DE. Architecture and membrane interactions of the EGF receptor. Cell 2013;152: 557–569.